River Flow 2010 - Dittrich, Koll, Aberle & Geisenhainer (eds) - © 2010 Bundesanstalt für Wasserbau ISBN 978-3-939230-00-7

Turbulence Structure in Bottom Layer of a Tidal Estuary

M. Razaz
Hydraulic & Coastal Engineering Laboratory, Dept. of Civil and Environmental Engineering, Hiroshima University, Kagamiyama 1-4-1, Higashi Hiroshima, 739-8527, Japan

K. Kawanisi
Dept. of Civil and Environmental Engineering, Hiroshima University, Kagamiyama 1-4-1, Higashi Hiroshima, 739-8527, Japan

ABSTRACT: Prediction of cohesive sediment concentration and its transport is vital to managers in coping with problems. Detailed measurements and processed data are necessary tools for development and application of this knowledge. In order to investigate turbulence structure in the bottom layer of a tidally dominated river a point at the center of the Ōta Floodway was selected to deploy instruments during 25 hours of Aug. 2008. Vertical profiles of turbulence parameters like Reynolds stress, eddy viscosity, and production/dissipation rates were obtained from the data collected by a HRCP. An ADV was deployed to measure velocity components near the bed. Using ADVs offers high quality point measurements of turbulence statistics. Density data was collected every hour throughout the water column by CTD casts. Temporal variations of turbulence statistics in two reference level as well as their vertical profiles are presented at this paper. A highly stratified layer in about 0.2 mab affected turbulence parameters like a free surface especially in slack waters. Stability function S_M and proportionality constant B_1 in Mellor-Yamada model was investigated and found to be different with suggested values in the original model.

Keywords: Estuaries, Turbulence, M-Y model, Acoustic Doppler effect.

1 INTRODUCTION

Aspect of cohesive sediment transport in estuaries is important to engineering projects including riverbank stability, residual onshore sediment transport, scouring around bridge piers, navigation, water quality and ecological problems. Saline water intrusion, stratification, tidal oscillation, river discharge, and wind driven waves among all turn estuarine areas too complex to be studied by laboratory methods. On the other hand, because of highly unsteady conditions it is difficult to conduct *in situ* measurements. Recently, devices based on the Doppler Effect referred to as pulse-to-pulse coherent Doppler sonar have been developed to collect *in situ* data with high precision throughout the water column to study small-scale processes, namely Kawanisi (2004) studied structure of turbulent flow in the Ōta River, Japan. Using the data collected by a high-resolution acoustic Doppler current profiler (HRCP), he examined turbulence statistics and density profiles. Also, stability function S_M in the M-Y model (Mellor and Yamada, 1982) was redefined by him. At present work, we performed observation for 25 hours at the center of the Ōta Floodway to study turbulent structure and suspended sediment transport in a tidally-dominated estuary during a complete tidal phase. For improving knowledge about the Y-M model parameters, we tried to define stability function and proportionality constant in a complete cycle of a semi-diurnal tide.

1.1 *Study Area and Observation Method*

Ōta Floodway is the westernmost branch of the Ōta River with a length of nearly 9 km that empties to the Hiroshima Bay. It is a tidally-dominated river where highest tidal range in an extreme spring tide can reach 4 m near the mouth. Fresh water inflow to this part of the river is controlled by the Gion Sluice Gates (Figure 1).

We operated a commercially-available high-resolution current profiler: HR-AquaDopp to measure velocity profile accurately, the HRCP was mounted downwardly on a special frame to

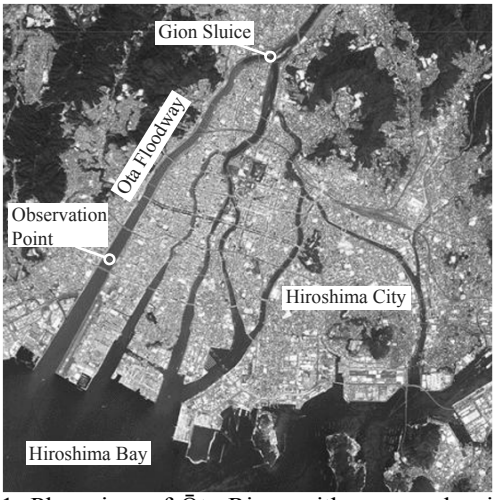

Figure 1. Plan view of Ōta River with surveyed point. It is likely that 10% of fresh water is diverted to the Ōta Floodway through the Gion Sluice gates.

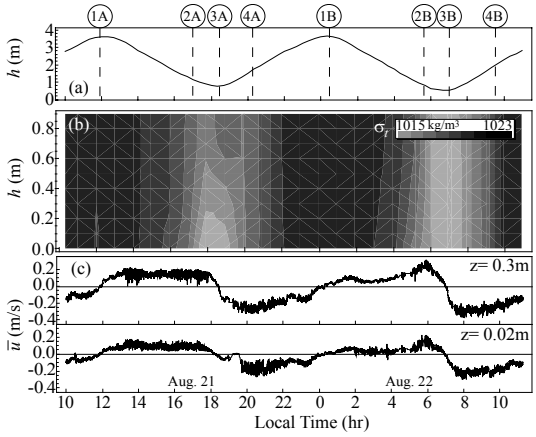

Figure 2. Temporal variations of (a) water depth, (b) density (σ_t) profile, and (c) streamwise velocity.

prevent device from being shaken. Data collected at 1.0 Hz sampling rate and 2.0 cm cell depth. HRCP distance from bed varied from 0.65 to 1.1 m above the bed (mab) in order to match horizontal velocity range of the HRCP with highest horizontal current speed. To measure turbulent velocity in the vicinity of the bed, the ADV with a synchronized tilt-compass sensor was fixed in about 8 cm far from the bed. ADV beams intersect at approximately 50 mm far from the center of sampling volume. A Compact CTD (conductivity-temperature-density) sensor developed by Alec Electronics was used to check salinity and density profiles every hour in 10-cm depth-triggered mode. Observation fulfilled through 21-22 Aug. 2008 using three described instruments in a point that is located 2.8 km far from the river mouth at the center of the river (Figure 1).

2 VELOCITY AND DENSITY PROFILES

The water depth variation ranged from 0.8 to 3.6 m during observation as shown in Figure 2(a). The depth-time variation of density is plotted in Figure 2(b). According to this plot, stratification changes can be attributed to tidal phase. Tidal straining and wind-driven currents are responsible for stratification variation as cited by Kawanisi (2004). Figure 2(c) shows temporal variations of streamwise velocity at 0.02 and 0.30 mab acquired from HRCP data. Usually, fast movement of particles in a turbulent field leads to low data correlation for acoustic Doppler sensors. This can be recognized as spiky velocity data in the following figures.

Velocity profiles during ebb follow logarithmic distribution for stratified flow and are expressed by the log-linear law:

$$\hat{u} = \frac{u_*}{\kappa}\left(\ln\frac{z}{z_0} + \beta\frac{z - z_0}{L}\right) \tag{1}$$

where $\hat{u}$= is the time averaged velocity, u_*= friction velocity, κ= von Karman's constant, z_0= roughness length, β= empirical constant, and L= Monin-Obukov length.

Critical condition for incipient motion of sediment is examined as below: according to Kawanisi (2004) and Kawanisi *et al.* (1996) we assumed during flood (ebb) phase β/L=0.025 (0.2) cm^{-1}, z_0= 5 mm, κ= 0.4. The results are presented in Figure 3. Hereafter, symbol "↑" stands for approximate HWS and "↓" for the approximate LWS in the figures. Critical Shields parameter θ_c is a well-known parameter for testing incipient motion of sediments and is defined as:

$$\theta_c = \frac{\tau_c}{(\rho_s - \rho_w)gd} = \frac{u_*^2}{sgd} \tag{2}$$

where, d= sediment particle diameter, g= gravitational acceleration, $s=\rho_s/\rho_w$-1= submerged specific weight of sediment, and ρ_s and ρ_w= densities of fluid and sediment, respectively. In order to calculate θ_c instead of using Shields diagram we can solve an equation that provides a satisfactory approximation (Cao *et al.*, 2006):

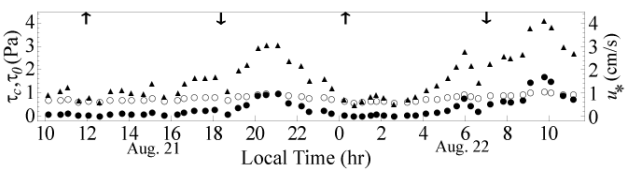

Figure 3. Temporal variations of critical shear stress (●), near-bed shear stress (○) and shear velocity (▲).

$$\ln\theta_c = -\ln R_* + 0.5003\ln\left[1 + \left(0.1359R_*\right)^{2.5795}\right] - 1.7148 \tag{3}$$

where, shear Reynolds number $R_*=u_*d/\nu$ and ν= kinematic viscosity of fluid. By solving Eq. (3) and replacing θ_c in Eq. (2) assuming s= 2.65, and d= 0.4 mm it is concluded that during observation critical shear stress τ_c was often more than currents induced shear stress τ_0. Subsequently most of small particles required for flocculation are supplied from Hiroshima Bay.

3 DEPTH-TIME VARIATION OF TURBULENCE

Figure 4 shows the depth-time variation of turbulence parameters derived from the HRCP data that are averaged over 5-minute intervals. Areas with absolute white color refer to the areas contain erroneous data. Figure 4(a) shows the Reynolds shear stress $-\overline{u'w'}$, where u and w are the current longitudinal and vertical velocities respectively and the prime denote fluctuation part. During the first ebb $|\overline{u'w'}|$ values were relatively higher than that of in the next ebb. In HWS, when the river is relatively calm the lowest Reynolds stresses can be detected. Usually, high turbulent kinetic energy TKE is associated with strong flood currents like on Aug. 21. Nevertheless, as it is illustrated in Figure 4(b) P_s reached its peak in ebb time on Aug. 22. Magnitude of P_s rarely exceeded unity. Lower amounts of $|\overline{u'w'}|$ resulted in undermost magnitudes of P_s during HWS. Negative values of P_s that are omitted from Figure 4(b) may be a correspondence to the sign reversal of $-\overline{u'w'}$ around the end of ebb, e.g. 4-6 p.m. of Aug. 21. Other incorrect data may be consequence of unreliable stress estimations or HRCP limitations in highly stratified flow. In Figure 4(c) variations of eddy viscosity coefficient K_M is plotted. Since it is a function of P_s and mean velocity gradients, maximal values of K_M are concurrent with P_s and or $-\overline{u'w'}$ peaks. Contrary to the first half of the tide, magnitudes of K_M in flood time are larger than that of during the ebb in the second tidal phase. During ebb time and particularly LWS, K_M had very small values near the bottom corresponding to weak near-bed-generated turbulence.

Figure 5 demonstrates temporal variations of turbulent velocity variables and resistance coefficient C_f at 0.02 and 0.26 mab. In this figure $\sigma_u=\left(\overline{u'^2}\right)^{1/2}, \sigma_w=\left(\overline{w'^2}\right)^{1/2}$.

Resistance coefficient can be evaluated from $\left|\overline{u'w'}\right| \Big/ \left(\int_{0.02}^{0.58}\overline{u}(z)dz/0.56\right)^2$, where $|\overline{u'w'}|_{0.02}$ is the absolute value of the Reynolds stress at 0.02 mab and $\overline{u}(z)$ is the averaged velocity over each 5 minutes. Values of plotted variables according to Mellor and Yamada (1982) in a neutral equilibrium boundary layer are defined as: $\sigma_u/u_*\approx 2$, $\sigma_w/\sigma_u\approx 0.5$, and $|\overline{u'w'}|/q^2\approx 0.15$. On the other hand, Nezu and Nakagawa (1987) showed that $|\overline{u'w'}|/q^2$ varies between 0.1 near the bed, reaches 0.04 near the water surface, and in the middle of water column is 0.15. σ_u/u_* obtained from HRCP data indicates average value of 3-4, neglecting dispersion in early hours of the observation. Figure 5 (b) reveals that σ_w/σ_u noticeably decreased in slack waters. Least values of $|\overline{u'w'}|/q^2$ were observed during water slacks with high stratification suggesting inactive and effectively irrotational part of turbulence was larger during those times. According to Bradshaw (1967) inactive part of turbulence doesn't produce any shear stress and is determined by the turbulence in the outer layer. This inactive motion is produced as a result of density interface in water column that acts like a free surface and suppresses the vertical movement of eddies.

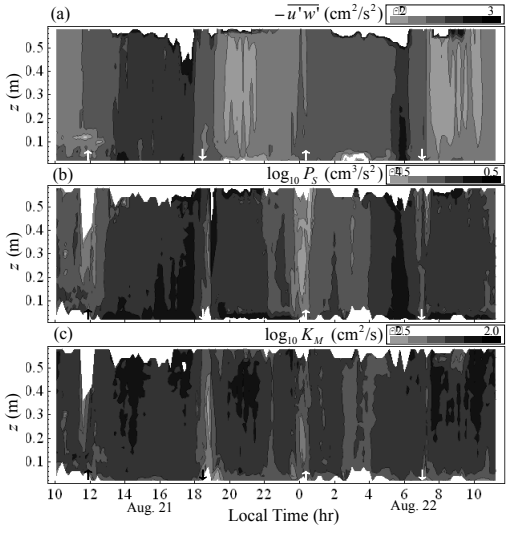

Figure 4. Depth-time distributions of (a) Reynolds stress, (b) shear production, and (c) eddy viscosity.

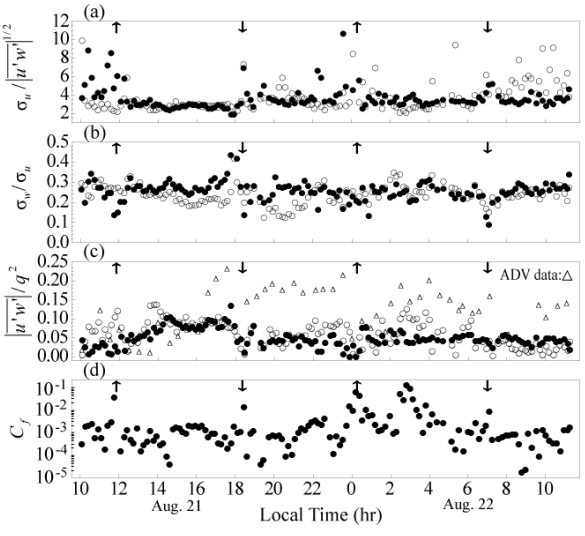

Figure 5. Temporal variations of turbulence parameters at 0.02 (○), and 0.26 mab (●).

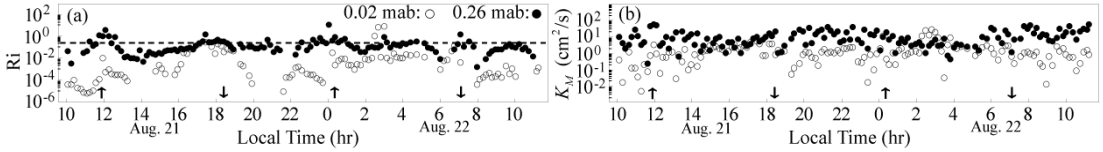

Figure 6. Temporal variations of (a) local gradient Richardson number, and (b) vertical eddy viscosity.

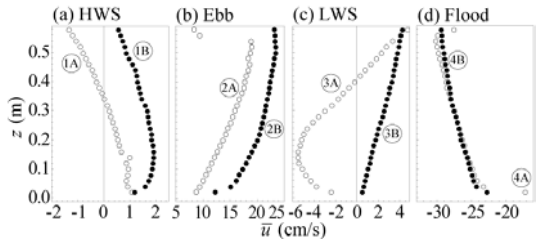

Figure 7. Vertical profiles of mean streamwise velocity.

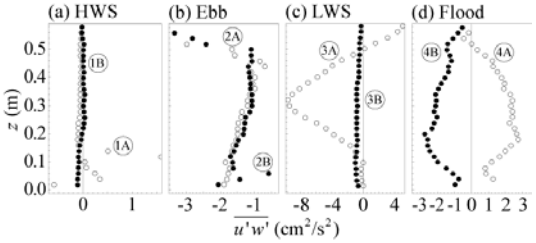

Figure 8. Vertical profiles of Reynolds shear stress.

Assuming turbulent length scale l= mixing length l_m, it is inferred that $|\overline{u'w'}|/q^2 = S_M^2$. According to Stacey *et al.* (1999) equivalency of l and l_m in stratified turbulent boundary layer is acceptable. Comparing Figures 5(c) and 2(a) reveals that S_M in the boundary layer can be a function of tidal phase. Highest (lowest) estimates of resistance coefficient C_f were recorded in ebb (flood) of Aug. 22. In Figure 6 temporal variations of Richardson number Ri and K_M are plotted at 2 reference levels of 0.02 and 0.26 mab, dash line stands for the critical value of Ri= ¼. Ri in the near-bottom layer rarely exceeds ¼, while large values of Ri could be found in upper layers during the first HWS/LWS. In Figure 6(b) temporal variations of eddy viscosity coefficient K_M are plotted. It seems that in upper layers K_M varies with tidal phase, i.e. higher values in flood and lowers in ebb are detectable. Near-bottom K_M reached its least values in HWS/LWS as a result of weak near-bed generated turbulence that stems from baroclinic pressure gradient.

4 VARIATIONS OF TURBULENCE ROFILES WITH TIDAL PHASE

Vertical profiles of mean velocity and a number of turbulence parameters are shown in Figures 7-11. Circulated numbers in each figure are referred to as tidal phase displayed in Figure 2(a). Also, letter "A" denotes the first and "B" the second semi-diurnal tide. In Figures 7(a)-(d) vertical distributions of the mean streamwise velocity are illustrated. During the first LWS shown in Figure 7 tidal straining can be recognized. In flood and ebb time, velocity profiles are logarithmic.

Reynolds shear stress profiles are plotted in Figure 8. Although, as cited before magnitudes of $|\overline{u'w'}|$ in the first ebb was larger than that in the second ebb, in the end of both ebbs $|\overline{u'w'}|$ seems almost identical. In calmer conditions, e.g. HWS, low values of $|\overline{u'w'}|$ are detectable. In flood time despite faster current speed, flow regime is not so turbulent in comparison with the first LWS. During the second LWS as a result of stratification, baroclinic pressure gradient and tidal straining, Reynolds shear stress reduced. In Figure 9 vertical distributions of vertical eddy viscosity is plotted. The sudden change in K_M profile during the first HWS around 0.15 mab is generated by high shear production at the same level.

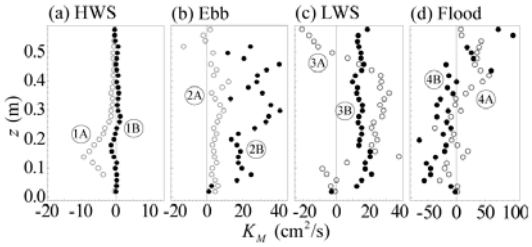

Figure 9. Vertical profiles of vertical eddy viscosity.

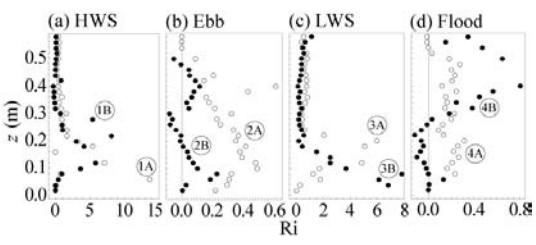

Figure 10. Vertical profiles of Richardson number.

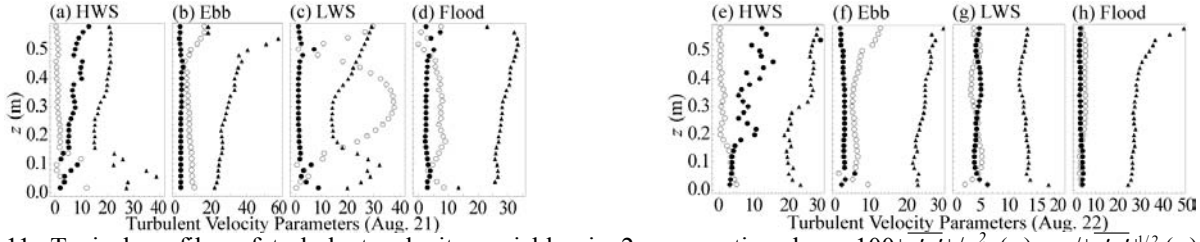

Figure 11. Typical profiles of turbulent velocity variables in 2 consecutive days: $100|\overline{u'w'}|/q^2$ (●), $\sigma_u/|\overline{u'w'}|^{1/2}$ (○), and $100\sigma_w/\sigma_u$ (▲) in both tidal cycles.

In the first ebb despite relative constant decrease of P_s with distance from the bed, vertical eddy viscosity profile was almost stable throughout water column. During LWS, especially (3A), we have different gradients of K_M with different signs. Such a phenomenon can be described as: in high stratification (Ri>0.5-0.7) buoyant production may cause vertical transfers of momentum and heat occur against their mean gradient (Komori *et al.*, 1983). As shown in Figure 10, Ri was excessively high in LWS/HWS that shows a highly-stratified and stable flow. Peak values of K_M were calculated in flood time.

S_M was almost stable through water column with tidal cycle except in HWS. Furthermore, stability function which is defined by $S_M = -\overline{u'w'}/q^2$ is more sensitive to turbulence energy q rather than Reynolds shear stress. This can be found by comparing Figures 5(c) and 11. concerning Figures 8 and 11, it Ratio of vertical velocity fluctuations to longitudinal fluctuation varied remarkably with tidal phase, i.e. largest values can be detected in flood and ebb times. Studies of Komori *et al.* (1983) showed that ratio of σ_w/σ_u decreases slightly as stratification shifts from neutral to weakly stable condition and then increases as Ri rises. Correspondingly in the first LWS when flow was stratified the Ri was high $\sigma_w > \sigma_u$. Rates of TKE production and dissipation ε are illustrated in Figure 12. We applied Kolmogorov's -5/3 power law to describe 1D kinetic energy density as a function of energy dissipation. Buoyant production P_b is estimated assuming K_M=K_H. Despite it is expected to measure largest magnitudes of P_s in flood time, peak values of shear production occurred in the first LWS with 0.5 cm^2/s^3 that is 2.5 times as large as that of in the flood. Most often buoyant production rate P_b is insignificant compared to P_s, though in the vicinity of stratified layer borders buoyancy rise to high scales. Since rate of energy dissipation is not equal to P_b+P_s except in HWS, we cannot assume a local balance of TKE according to dissipation obtained from HRCP. In order to make sure about the method and hardware applied to obtain TKE production/dissipation, we conducted short-term measurements in a laboratory flume using the same HRCP. Results notify an acceptable agreement between kinetic energy production and dissipation. Therefore, such an imbalance that was previously reported by Kawanisi (2004) and also studied by Stacey *et al.* (1999) may stem from unsteady state of flow during tidal cycles.

5 PARAMETERS OF M-Y MODELS

Vertical eddy viscosity K_M as a function of ql_m at 0.02 and 0.26 mab for the ebb and flood phase is plotted in Figure 13. Apparently K_M and ql_m are in good proportion, and if we accept that l=l_m then the ratio of K_M/ql_m will represent the amount of M-Y stability function S_M. Referring to Figure 5 (c) implies that stability function in ebb is larger than that in flood. As shown in Figure 13 highest values of stability function are limited to 0.29 and on average S_M≈0.25. Kawanisi (2004) calculated the highest value of S_M= 0.29 during flood in the Ōta Floodway. The assumption of neutral condition in M-Y model under which S_M is calculated is not valid because under unstratified equilibrium conditions Gulperin's function (Gulperin *et al.*, 1988) gives S_M=0.39 that is larger than estimated value of 0.29. Figure 14 is the scatter diagram of ε which is estimated from u-spectra against q^3/l_m. In M-Y model B_1=16.6, though here B_1 is notably larger. Assuming ε=P_b+ P_s, B_1 could be roughly estimated as 55. Kawanisi (2004) calculated this constant about 40 assuming ε=P_s.

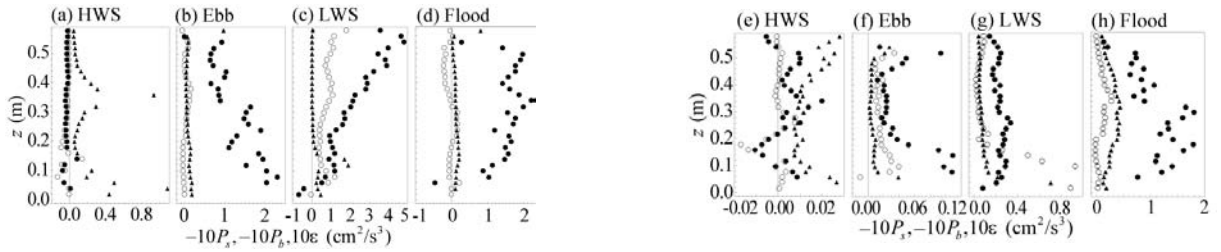

Figure 12. Typical profiles of turbulent energy production and dissipation rate: -10P_s (○), -10P_b (●), and ε (▲) in Aug. 21 (a)-(d) and Aug. 22 (e)-(h).

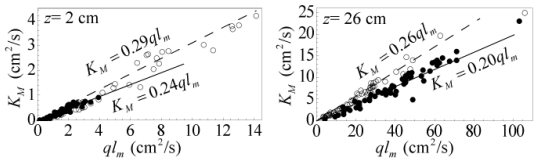

Figure 13. Relation between ql_m and K_M in ebb (○) and flood (●).

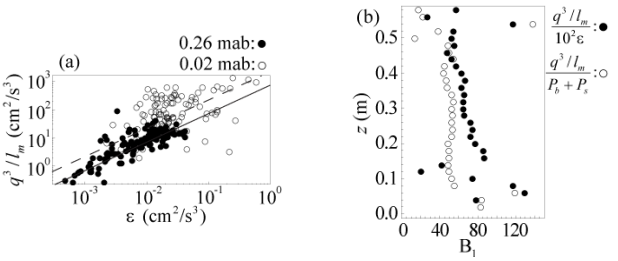

Figure 14. (a) Scatter diagram of energy dissipation rate against q^3/l_m, (b) vertical profile of constant B_1.

6 CONCLUSIONS

Examining critical and current-induced shear stress suggests that just over flood phase resuspension happens in the observation site. A high turbulent current at the first ebb deeply affected the results, i.e. largest values of $|u'w'|$ and P_s was detected in ebb time, however K_M reached its peak during flood. During HWS/LWS flow became highly stratified especially in lower layers. σ_u/u_* found to be approximately 3 showing no relation with tidal phase except HWS. Least values of $|u'w'|/q^2$ were observed in relatively slack waters that means inactive and effectively irrotational part of turbulence was larger during LWS and HWS. Stability function in M-Y model S_M calculated as approximately 0.2 in flood and 0.3 over ebb time. Constant B_1 evaluated as 55 which is quite larger than previous studies as a result of imbalance in TKE production and dissipation. This imbalance implies that for estimating turbulent parameters equality of production and dissipation rates is unreliable.

REFERENCES

Bradshaw, P. 1967. Inactive motion and pressure fluctuations in turbulent boundary layers, J. Fluid Mech., 30, 241-258.

Cao, Z., Pender, G., and Meng, J. 2006. Explicit Formulation of Shields Diagram for Incipient Motion of Sediment, J. Hydraulic Engineering, ASCE, 132(10), 1097-1099.

Gulperin, B., Kantha, L., Hassid, S., and Rosati, A. 1988. A quasi-equilibrium turbulent energy model for geophysical flows, J. Atmos. Sci., 45(1), 55-62.

Kawanisi, K. (2004). Structure of turbulent flow in a shallow tidal estuary, J. of Hydraulic Engineering, ASCE, 130(4), 360-370.

Kawanisi, K., Tsutsui, T., Nakamura, S., and Nishimaki, H. 1996. Influence of Tidal Range and River Discharge on Transport of Suspended Sediment in the Ohta Floodway, J. Hydrosciences and Hydraulic Engineering, 24(1), 1-9.

Komori, S., Ueda, H., Ogino, F., and Mizushima, T. 1983. Turbulence structure in stably stratified open-channel flow, J. Fluid Mechanics, 130, 13-26.

Mellor, G.L., and Yamada, T. 1982. Development of a turbulence closure model for geophysical fluid problems, Rev., Geophys. Space Phys., 20(4), 851-875.

Nezu, I. and Nakagawa, H. 1987. Turbulence in open-channel flows, Balkema, Rotterdam, The Netherlands, 281, 1987.

Stacey, M.T., Monismith, S.G., and Burau, J.R. 1999 Observation of turbulence in a partially stratified estuary, J. Phys. Oceanogr., 129, 1950-1970.

Stone, M. C., and Hotchkiss, R. H. 2007 Evaluating velocity measurement techniques in shallow streams, J. Hydraulic Research, 45(6), 752–762.